Biomarker Evidence for Photosynthesis During Neoproterozoic Glaciation

Alison N. Olcott,[1]* Alex L. Sessions,[2] Frank A. Corsetti,[1] Alan J. Kaufman,[3] Tolentino Flavio de Oliviera[4]

Laterally extensive black shales were deposited on the São Francisco craton in southeastern Brazil during low-latitude Neoproterozoic glaciation ~740 to 700 million years ago. These rocks contain up to 3.0 weight % organic carbon, which we interpret as representing the preserved record of abundant marine primary productivity from glacial times. Extractable biomarkers reflect a complex and productive microbial ecosystem, including both phototrophic bacteria and eukaryotes, living in a stratified ocean with thin or absent sea ice, oxic surface waters, and euxinic conditions within the photic zone. Such an environment provides important constraints for parts of the "Snowball Earth" hypothesis.

The impacts of low-latitude Neoproterozoic glaciation on the biosphere are widely debated (*1*–*6*). On one hand, one conception of "Snowball Earth" envisions sea-ice cover thick enough to preclude photosynthesis over most of the Earth, creating an "intense environmental filter" for the survival of photosynthetic organisms (*2*). Thick ice cover would also lead to anoxic oceans, threatening the existence of all eukaryotes. In this model, photosynthetic and eukaryotic clades survived in rare refugia, perhaps sustained by hydrothermal or volcanic activity or in transient equatorial polynya. Thus, the Neoproterozoic glaciations would have represented major evolutionary bottlenecks that influenced the subsequent radiation of multicellular life (*2*, *5*, *7*–*9*). Large ^{13}C depletions in the carbonate rocks that cap the glacial deposits have been attributed to the collapse of biologic productivity (and its consequent isotopic fractionation) during these glaciations (*2*, *9*). On the other hand, some climate models indicate that tropical oceans could have persisted through the glaciations with thin or no sea ice, allowing enough sunlight to reach the oceans to sustain diverse marine ecosystems and providing less extreme evolutionary pressure (*10*, *11*). Unfortunately, the results of these climate models are sensitive to several parameters that are difficult to estimate, including CO_2 concentration, oceanic heat transport, the flux of windborne dust, snow thickness and distribution, and ice optical properties (*11*). Both hypotheses remain speculative, because no unambiguous proxy for sea ice thickness is available. Here, we describe organic-rich shales deposited in southeastern Brazil during a Neoproterozoic glaciation. Given their lateral extent [>1000 km^2 (*12*)], substantial organic content (up to 3.0%), and stratigraphic position within the midst of glacial diamictites, these rocks provide evidence that life continued to flourish, at least in this location, during low-latitude Neoproterozoic glaciation.

Samples were collected from a subsurface core drilled near Paracatú, Brazil (Fig. 1A), in the Neoproterozoic Vazante Group by the Companhia Mineira de Metais (*13*). The succession (Fig. 2) includes the Serra do Garrote Formation, the glacial Poço Verde and Morro do Calcario formations, and the Lapa Formation, recently recognized as a postglacial succession from carbon- and sulfur-isotopic anomalies at its base (*14*). In the Paracatú region, the Poço Verde Formation includes diamictite, rhythmic marl, carbonate, and thinly laminated organic-rich black shale, deposited below storm wave base. Although radiometric age constraints for the succession are unavailable, the strontium isotope composition of carbonate above the studied shale horizon (*15*) is consistent with an age of 740 to 700 million years (Ma) (*1*, *16*).

[1]Department of Earth Sciences, University of Southern California, Los Angeles, CA 90089, USA. [2]California Institute of Technology, Pasadena, CA 91125, USA. [3]University of Maryland, College Park, MD 20742, USA. [4]Companhia Mineira de Metais, Brazil.

*To whom correspondence should be addressed. E-mail: olcott@usc.edu

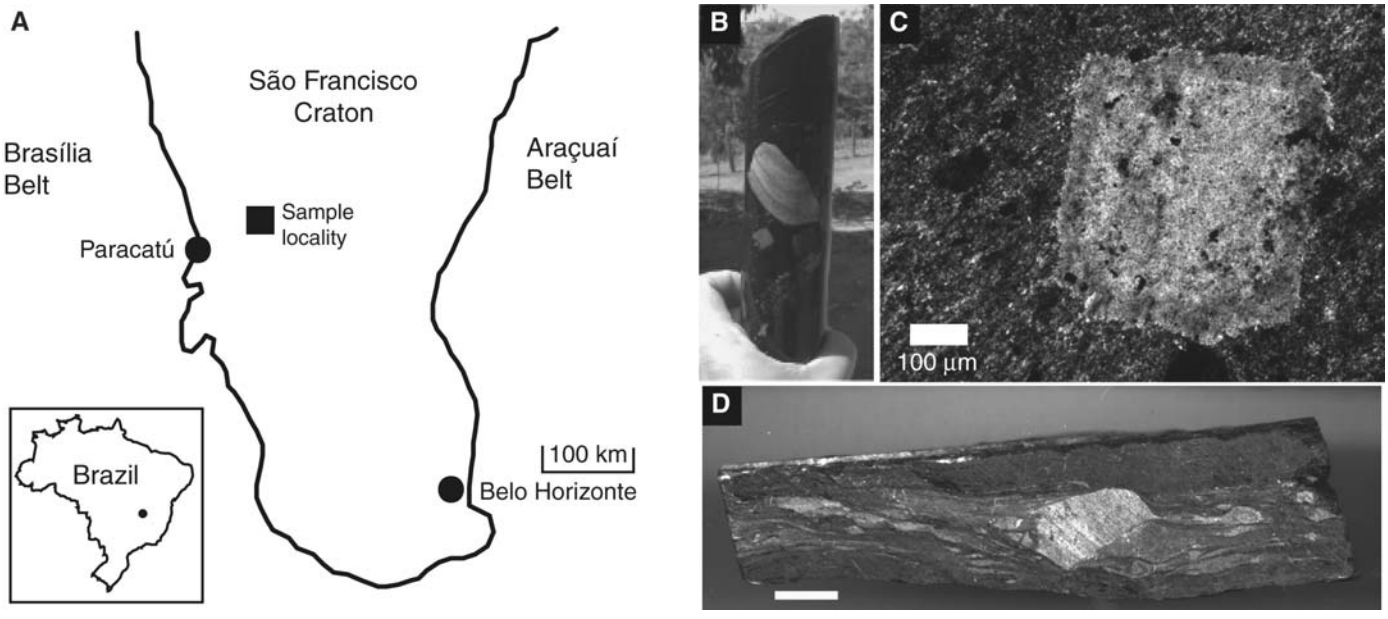

Fig. 1. (**A**) Locality map [modified after (*47*)] indicating the position of largely undeformed Vazante Group strata on the São Francisco craton between the Brasília and Araçuaí fold belts. (Inset) Brazil; dot marks region of interest. (**B**) Dropstone in core MAF 42-88 from the Neoproterozoic Poço Verde Formation. (**C**) Photomicrograph of carbonate nodule with squared crystal terminations formed before substantial compaction interpreted to be glendonite, a pseudomorph of ikaite formed in frigid, organic-rich sediments. (**D**) Faceted dropstone in core penetrating underlying laminae; scale bar is 5 mm.

Evidence for glacial processes exists throughout the Poço Verde Formation. Thinly laminated shale is sandwiched between thick carbonate diamictites, and lonestones, interpreted as ice rafted debris (dropstones), are present within it, indicating the presence of overlying ice at the time of deposition (Fig. 1, B and D). Shale samples also contain small nodules with squared prismatic crystal terminations formed before substantial compaction, which we identify as glendonite (Fig. 1C). Glendonite is a pseudomorph after ikaite, a carbonate mineral that most commonly forms between –1.9° and 7°C in organic-rich muds and that has been previously reported in a Neoproterozoic glacial succession from Svalbard containing "wispy" organic matter (*17*). It is probable that Poço Verde Formation strata were deposited at relatively low latitudes. The São Francisco craton, upon which the Poço Verde strata were deposited, was contiguous with the Congo craton in southern Africa, which contains broadly equivalent glacial deposits with near-equatorial paleolatitudes (*3*). In sum, the features recorded in the Poço Verde Formation of the Vazante Group are consistent with deposition at relatively low latitudes during Neoproterozoic glaciation.

We consider first the possibility that the organic-rich shale might represent recycled sediments that were eroded and redeposited via glacial processes. Several lines of evidence argue against this interpretation. Dropstones in the black shale are almost exclusively composed of organic-poor carbonate, indicating that the terrain eroded by the glaciers was not rich in black shale. Ikaite (the precursor to observed glendonite) forms in cold, anoxic sediments where rapid microbial remineralization of organic matter dramatically boosts porewater concentrations of both alkalinity and orthophosphate, a calcite inhibitor (*18*). Finely disseminated pyrite is also abundant in the matrix of the black shales, presumably resulting from extensive remineralization of organic matter by sulfate-reducing bacteria. Organic matter in eroded black shales is widely observed to be recalcitrant to microbial degradation (*19*) and thus would not have supported conditions necessary for either ikaite or sulfide formation. Therefore, we conclude that the preserved organic matter is the remains of abundant primary productivity occurring during the glacial interval.

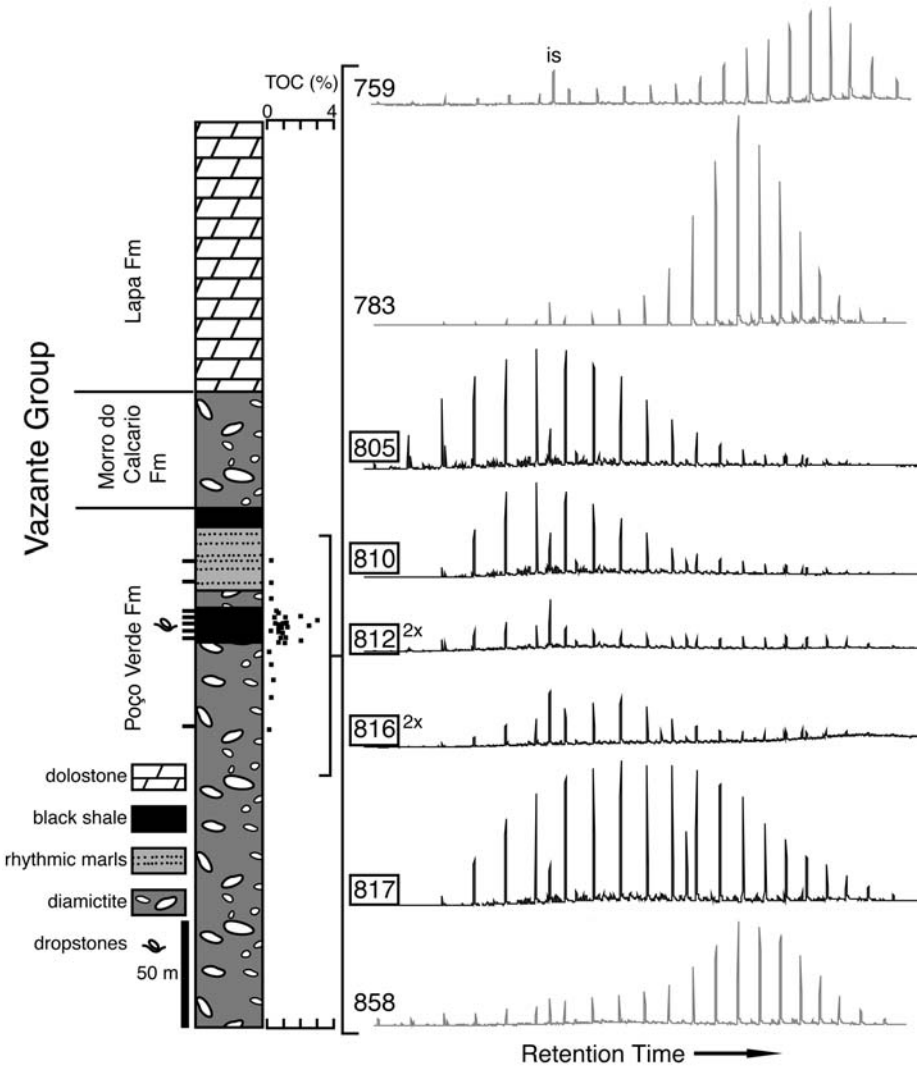

Fig. 2. Stratigraphic log of the core, TOC through the Poço Verde Formation (Fm), and GC-MS total ion chromatograms for saturate fractions of extracted samples. The underlying Serra do Garrote Formation was not sampled by this drill core, but in other cores the Poço Verde Formation is over 200 m thick. Tick marks to the left of the core log show location of samples used for biomarker analysis, and the numbers to the left of the chromatograms show the depth from which these samples were taken. The five boxed depths indicate samples from the organic-rich interval, which were also used to determine the biomarker ratios in table S2. IS is internal standard (hexadecanoic acid isobutylester), present in all chromatograms. Chromatograms for meters 812 and 816 are shown at 2× vertical scale.

To further evaluate environmental conditions during deposition of the Poço Verde Formation, we examined extractable biomarkers in the organic-rich shale by standard techniques (*20*). This interval is located 100 m below the postglacial unit and bounded above and below by diamictite units, and was thus deposited during the glaciation. Although these rocks are well preserved in comparison to other syn-glacial deposits of similar age, they are thermally mature and contain very small quantities of bitumen. They are thus susceptible to interference from migrating hydrocarbons, drill-core collection and handling, and extant biota. Although these sources of contamination would not contribute substantially to measured total organic carbon (TOC, which is >99% insoluble kerogen), they could affect biomarker distributions.

Multiple lines of evidence support the interpretation that extractable biomarkers in these rocks are indigenous. (i) Samples were repeatedly crushed and extracted, and the highest yields of biomarkers were obtained from the finest-grained powders (i.e., the final extraction). (ii) TOC contents and carbon-isotope ratios of kerogen and bitumen covary with lithology. Extract yields from different rocks correlate with measured TOC and constitute <0.05% of the TOC (table S1). (iii) Extracts from carbonate rocks above the organic-rich intervals and from diamictites below contain different biomarker distributions than those within organic-rich rocks (Fig. 2 and fig. S1), whereas laboratory blanks contained no detectable biomarkers. (iv) No petroleum source rocks or reservoirs are known from the Paracatú region, and no biomarkers indicative of exclusively Phanerozoic biota (such as higher plants) were detected. (v) Biomarker ratios that are controlled by depositional source conditions vary between rock types (table S2). (vi) Biomarker

ratios controlled by heating (table S2) predict moderate thermal maturity in these rocks, in agreement with petrologic assessments of thermal history including amber-colored blebs of organic matter. (vii) Polar lipids indicative of living microorganisms were not detected in the extracts.

Biomarker abundance is higher in the black shale than in the marl and the carbonate-matrix diamictite (fig S1). Taxa-specific biomarkers (table S3) extracted from the syn-glacial organic-rich shale include 2-α-methylhopanes, derived from cyanobacteria (*21*), and alkylated 2,3,6-trimethylbenzenes, which we interpret as molecular fossils of the isoprenoid pigment isorenieratene from green sulfur bacteria (*22*, *23*). The green sulfur bacteria are anaerobic organisms that use H_2S as the electron donor for photosynthesis and are strongly inhibited by the presence of O_2. Their presence is generally interpreted as evidence for an anoxic, sulfidic, photic zone (*22*). These biomarkers provide good evidence for the presence of photosynthetic organisms and, by extension, the penetration of sunlight to the sea surface. Other extractable biomarkers include 3-β-methylhopanes, known only from microaerophilic proteobacteria including the aerobic methanotrophs (*24*). Gammacerane, a C_{30} triterpane, is thought to derive from protozoan tetrahymanol (*25*). Although the organisms that produce tetrahymanol are heterotrophic aerobes, gammacerane is often prevalent in sediments formed under a stratified water column. Stable carbon-isotope studies of gammacerane have shown that the bacteriovores that produce tetrahymanol consume green and purple sulfur bacteria, so the protozoa live at or below the chemocline (*26*). C_{27} and C_{28} di- and trinorhopanes tend to be found in high concentration in sulfidic sediments, although the precursor organism is not yet known (*27*). Steranes not methylated at C-4, also found in the core, are produced exclusively by aerobic eukaryotes and may represent algal contributions.

Taken together, the biomarker data portray a diverse microbial community based upon photosynthetic primary production, consistent with sunlight availability and thus with relatively thin sea ice or an ice-free environment. Residents included anaerobic and aerobic bacteria, photoautotrophs and heterotrophs, eukaryotes, and perhaps even protists. Although our description of such a community via molecular fossils is necessarily incomplete and has very limited ability to discern eukaryotic diversity, the assemblage is nevertheless indistinguishable from those recorded in rocks both before and after this low-latitude Neoproterozoic glaciation (*27–32*). There is thus no evidence of a biotic crisis among prokaryotes at this location, and the inferred oxic, sunlit waters would have provided ample habitat for eukaryotes. Recent investigations of syn-glacial microfossil assemblages have reached similar conclusions (*33*, *34*).

Although the Poço Verde Formation rocks are consistent with local ice-free conditions, they are also compatible with the possibility that a complex ecosystem persisted within or immediately beneath relatively thin sea ice. Both modern and ancient examples of productive sea ice are known. Permian glacial strata in Tasmania provide a Paleozoic analog and contain up to 60% organic carbon interbedded with abundant ice-rafted debris (*35*). Perhaps the most striking modern analog originates in the highly productive ice margin environments surrounding Antarctica today, where complex communities of microbial eukaryotes (including metazoa) and photosynthetic and heterotrophic bacteria thrive (*36–39*). Annual net primary productivity in the Ross Sea is estimated at 200 g C m^{-2} $year^{-1}$ (*40*), comparable to estimates for coastal oceans of 250 g C m^{-2} $year^{-1}$ (*41*). Such environments have been previously proposed as analogs to Snowball Earth (*39*, *42*). The Poço Verde strata described here provide some support for this proposal.

Whether the environment represented by the Poço Verde rocks represents a singular, albeit large, refugium or a widespread phenomenon remains an open question to be settled by discovery and analysis of other rocks. The Poço Verde strata suggest limited ice thickness at low latitudes during at least part of the glacial interval, although the data are compatible with periods of more complete ice cover at other times. However, if the Poço Verde strata are representative of more widespread conditions, then the hypothesis of thick, global sea ice—and dependent mechanisms for carbon-isotopic anomalies during this period—will need to be reexamined. Regardless of the extent to which the Earth was icebound, the presence of this deposit indicates that diverse life, including eukaryotes and photosynthetic bacteria, apparently continued in abundance during this Neoproterozoic glaciation.

References and Notes

1. A. J. Kaufman, A. H. Knoll, G. M. Narbonne, *Proc. Natl. Acad. Sci. U.S.A.* **94**, 6600 (1997).
2. P. F. Hoffman, A. J. Kaufman, G. P. Halverson, D. P. Schrag, *Science* **281**, 1342 (1998).
3. M. J. Kennedy, N. Christie-Blick, L. E. Sohl, *Geology* **29**, 443 (2001).
4. M. J. Kennedy, N. Christie-Blick, A. R. Prave, *Geology* **29**, 1135 (2001).
5. P. F. Hoffman, D. P. Schrag, *Terra Nova* **14**, 129 (2002).
6. F. A. Corsetti, A. J. Kaufman, *Geol. Soc. Am. Bull.* **115**, 916 (2003).
7. S. Xiao, in *The Extreme Proterozoic: Geology, Geochemistry, and Climate*, G. Jenkins, M. McMenamin, L. Sohl, Eds. [*Geophys. Monogr. Am. Geophys. Union* 146 (2004)], pp. 199–214.
8. J. L. Kirschvink, in *The Proterozoic Biosphere: A Multidisciplinary Study*, J. W. Schopf, C. Klein, Eds. (Cambridge Univ. Press, Cambridge, 1992), p. 1348.
9. B. Runnegar, *Nature* **405**, 403 (2000).
10. W. T. Hyde, T. J. Crowley, S. K. Baum, W. R. Peltier, *Nature* **405**, 425 (2000).
11. D. Pollard, J. F. Kasting, *J. Geophys. Res.* **110**, C07010 (2005).
12. M. Babinski, L. V. S. Monteiro, A. H. Fetter, J. S. Bettencourt, T. F. Oliveira, *J. S. Am. Earth Sci.* **2005**, 293 (2005).
13. Six cores were examined in the field, four of which were collected. One core was selected for biomarker analysis on the basis of the thickness of the black shale unit.
14. K. B. Brody, A. J. Kaufman, J. L. Eigenbrode, G. D. Cody, paper presented at the Geological Society of America Annual Meeting, Denver, CO, 7 to 10 November, 2004.
15. K. Azmy *et al.*, *Precambrian Res.* **112**, 303 (2001).
16. S. B. Jacobsen, A. J. Kaufman, *Geochim. Cosmochim. Acta* **161**, 37 (1999).
17. G. P. Halverson, A. C. Maloof, P. F. Hoffman, *Basin Res.* **16**, 297 (2004).
18. N. P. James, G. M. Narbonne, R. W. Dalrymple, T. K. Kyser, *Geology* **33**, 9 (2005).
19. J. I. Hedges, R. G. Keil, *Mar. Chem.* **49**, 137 (1995).
20. Information on materials and methods is available on *Science* Online.
21. R. E. Summons, L. L. Jahnke, J. M. Hope, G. A. Logan, *Nature* **400**, 554 (1999).
22. R. E. Summons, T. G. Powell, *Geochim. Cosmochim. Acta* **51**, 557 (1987).
23. Trimethylbenzes were identified from their mass spectra (fig. S2). Although they are widely interpreted as products of isorenieratene [e.g., (*43–45*)], one recent report (*46*) has suggested they might also be derived from β-carotene. Biomarker yields are too low to allow confirmatory compound-specific ^{13}C analyses.
24. R. E. Summons, L. L. Jahnke, in *Biological Markers in Sediments and Petroleum: A Tribute to Wolfgang K. Seifert*, J. M. Moldowan, P. Albrecht, R. P. Philp, Eds. (Prentice Hall, Englewood Cliffs, NJ, 1992), pp. 182–200.
25. H. L. ten Haven, M. Rohmer, J. Rullkoetter, P. Bisseret, *Geochim. Cosmochim. Acta* **53**, 3073 (1989).
26. J. S. Sinninghe Damste *et al.*, *Geochim. Cosmochim. Acta* **59**, 1895 (1995).
27. R. E. Summons *et al.*, *Geochim. Cosmochim. Acta* **52**, 2625 (1988).
28. R. E. Summons, M. R. Walter, *Am. J. Sci.* **290-A**, 212 (1990).
29. G. A. Logan, R. E. Summons, J. M. Hayes, *Geochim. Cosmochim. Acta* **61**, 5391 (1997).
30. G. A. Logan *et al.*, *Geochim. Cosmochim. Acta* **63**, 1345 (1999).
31. K. Arouri, P. J. Conaghan, M. R. Walter, G. C. O. Bischoff, K. Grey, *Precambrian Res.* **100**, 235 (2000).
32. C. Li, P. a. Peng, G. Sheng, J. Fu, Y. Yan, *Precambrian Res.* **125**, 337 (2003).
33. F. A. Corsetti, S. M. Awramik, D. Pierce, *Proc. Natl. Acad. Sci. U.S.A.* **100**, 4399 (2003).
34. F. A. Corsetti, A. N. Olcott, C. Bakermans, *Palaeogeogr. Palaeoclimatol. Palaeoecol.*, in press.
35. A. T. Revill *et al.*, *Geochim. Cosmochim. Acta* **58**, 3803 (1994).
36. J. C. Priscu *et al.*, *Science* **280**, 2095 (1998).
37. D. R. Mueller, W. F. Vincent, W. H. Pollard, C. H. Fritsen, *Nova Hedwigia Beih.* **123**, 173 (2001).
38. D. N. Thomas, G. S. Dieckmann, *Science* **295**, 641 (2002).
39. W. F. Vincent, D. R. Mueller, S. Bonilla, *Cryobiology* **48**, 103 (2004).
40. W. O. Smith Jr., L. I. Gordon, *Geophys. Res. Lett.* **24**, 233 (1997).
41. G. A. Knauer, in *Interactions of C, N, P, and S Biogeochemical Cycles and Global Change*, R. Wollast, F. T. Mackenzie, L. Chou, Eds. (Springer-Verlag, New York, 1993), pp. 211–231.
42. W. F. Vincent *et al.*, *Naturwissenschaften* **87**, 137 (2000).
43. D.-J. H. Simons, F. Kenig, C. J. Schroder-Adams, *Org. Geochem.* **34**, 1177 (2003).
44. T. C. Brown, F. Kenig, *Palaeogeogr. Palaeoclimatol. Palaeoecol.* **215**, 59 (2004).
45. K. Grice *et al.*, *Science* **307**, 706 (2005); published online 20 January 2005 (10.1126/science.1104323).
46. M. P. Koopmans *et al.*, *Geochim. Cosmochim. Acta* **60**, 4467 (1996).
47. T. R. Fairchild *et al.*, *Precambrian Res.* **80**, 125 (1996).

48. We thank Companhia Mineira de Metais for samples,

R. Summons and E. Grosjean for helpful discussion and metastable-reaction monitoring gas chromatography–mass spectroscopy (GC-MS) analyses; G. Love, A. Bradley, J. Brocks, C. Li, M. Eek, K. Nealson, and W. Berelson for helpful discussion; J. Pinho and K. B. Brody for help in Brazil; N. Geboy and C. France for TOC abundance data; G. McDonald for lab access; as well as two anonymous reviewers for comments.

Supported by NSF grants EAR0418083 (F.C., A.S., A.O.) and EAR0126378 (A.J.K.) and NASA Exobiology grant 42000-62153 (F.C. and A.O.).

Supporting Online Material
www.sciencemag.org/cgi/content/full/1115769/DC1
Analytical Methods
Figs. S1 and S2
Tables S1 to S3
References and Notes

6 June 2005; accepted 21 September 2005
Published online 29 September 2005;
10.1126/science.1115769
Include this information when citing this paper.

The Evolution of Titan's Mid-Latitude Clouds

C. A. Griffith,[1] P. Penteado,[1] K. Baines,[2] P. Drossart,[3] J. Barnes,[1] G. Bellucci,[4] J. Bibring,[5] R. Brown,[1] B. Buratti,[2] F. Capaccioni,[6] P. Cerroni,[6] R. Clark,[7] M. Combes,[3] A. Coradini,[6] D. Cruikshank,[8] V. Formisano,[4] R. Jaumann,[9] Y. Langevin,[5] D. Matson,[2] T. McCord,[10] V. Mennella,[11] R. Nelson,[2] P. Nicholson,[12] B. Sicardy,[3] C. Sotin,[13] L. A. Soderblom,[14] R. Kursinski[1]

Spectra from Cassini's Visual and Infrared Mapping Spectrometer reveal that the horizontal structure, height, and optical depth of Titan's clouds are highly dynamic. Vigorous cloud centers are seen to rise from the middle to the upper troposphere within 30 minutes and dissipate within the next hour. Their development indicates that Titan's clouds evolve convectively; dissipate through rain; and, over the next several hours, waft downwind to achieve their great longitude extents. These and other characteristics suggest that temperate clouds originate from circulation-induced convergence, in addition to a forcing at the surface associated with Saturn's tides, geology, and/or surface composition.

The atmosphere of Saturn's largest moon, Titan, contains methane, which, like water on Earth, can exist as a gas, ice, and liquid. This moon is hypothesized to resemble Earth, with a methane cycle similar to the terrestrial hydrological cycle, involving methane clouds, rain, and surface liquids. Yet, unlike Earth, only two kinds of clouds have been detected recently on Titan: large storms near the south pole and long clouds predominantly at –40° latitude (*1*–*8*). The south polar clouds reside at the altitude of neutral buoyancy (*2*, *3*), which is indicative of convection (*5*). Their morphologies and Titan's recent south summer solstice (during October 2002) suggest a seasonal explanation for their formation, through a polar updraft resulting from Titan's pole-to-pole circulation and dynamical lifting from surface heating (*3*, *9*, *10*). The narrow mid-latitude clouds, observed between –37° and –44° latitude, extend several hundred to several thousand kilometers in longitude, residing primarily at 0° ± 40° and secondarily at 90° ± 40° west longitude (*4*). The clouds' propensity for particular spots on Titan's disk suggests a tie to the surface (*4*). Yet Cassini images do not display the morphologies expected of orographic clouds nor the dark and uniform appearance expected of seas (*11*, *12*) that would suggest marine clouds. Cloud formation through methane volcanic outgassing could explain the large amounts of methane in Titan's atmosphere (despite its photochemical loss rate of $\sim 6 \times 10^7$ kg/day), in addition to the temperate clouds' locations. However, the volcanoes would have to coincidentally reside at –40° latitude or outgas sufficient methane to instigate widespread deep convection. The longitude most preferred by the mid-latitude clouds coincides with the sub-Saturn point, which experiences large variations in pressure as Titan orbits Saturn (*13*). However, there has been no observed correlation with cloud activity and Titan's orbital position. Alternatively, Titan's general circulation may give rise to latitudinally confined clouds. Yet this answer does not explain the clouds' preferences for certain longitudes. Here we present measurements from the Cassini Visual and Infrared Mapping Spectrometer (VIMS) (*14*) of the structure and evolution of Titan's clouds, which are diagnostic of the physical processes that govern their formations.

Six spectral images of Titan's clouds were recorded by VIMS on 13 December 2004 as Cassini approached Titan on the third (TB) flyby, from a distance of 236,000 to 179,000 km (Fig. 1). The pixel resolution of the clouds ranged from 90 to 130 km and 50 to 70 km in the roughly east-west and north-south directions, respectively, with the highest resolutions achieved in the last image recorded during the 3-hour sequence. Each pixel within the images consists of a spectrum from 0.8 to 5.0 μm, with a resolving power of 143 at 2 μm. Our analysis focuses on the 2- to 2.5-μm section of the spectra that, as a result of variable methane absorption, samples Titan's atmosphere from 100 km to the surface. Within the center of the methane bands (at 2.25 μm), Titan's atmosphere is opaque and sunlight is reflected from the stratosphere, at roughly 100 km altitude. Between the methane bands (at 2.0 μm), Titan's atmosphere is fairly transparent and sunlight reaches the surface. At intermediate wavelengths (2.12 to 2.16 μm), sunlight probes Titan's troposphere at 10 to 40 km, where methane condenses (*1*). Hourly variations in Titan's 2.12- to 2.16-μm albedos occur solely as a result of changes in the opacity of clouds in the middle to upper troposphere (*1*, *5*). Four mid-latitude clouds are readily identified in the six VIMS images. They reside at the latitude and longitude coordinates of [–61:134], [–47:157], [–43,176], and [–41,115] and are referenced as cloud 1 through cloud 4, respectively (Fig. 1).

We approximate the radiative transfer equation with the discrete ordinates algorithm to simulate the absorption and scattering of Titan's atmosphere and surface (*15*). Comparing the calculated spectra to the data, we estimate the optical depths of the stratospheric haze and methane clouds, the cloud altitudes, and surface reflectivity. Methane, the primary absorber, is calculated from line-by-line techniques, using parameters from the HITRAN database (*16*) and assuming a Voigt line profile and the Voyager temperature profile (*17*). We also include pressure-induced absorption (*18*) due to H_2 and N_2. We assume a methane relative humidity of 50% (0.088 mixing ratio) at the surface and a constant mixing ratio (0.017) in the stratosphere (*19*, *20*). A constant methane mixing

[1]Lunar and Planetary Laboratory, University of Arizona, Tucson, AZ 85721, USA. [2]Jet Propulsion Laboratory, California Institute of Technology, Pasadena, CA 91109, USA. [3]Observatoire de Paris, 5 Place Jules Jannsen, Meudon, France. [4]Instituto di Fisica dello Spazio Interplanetario, Consiglio Nationale delle Richerche (CNR), Rome, Italy. [5]Institut d'Astrophysique Spatiale, Université de Paris-Sud, Orsay, France. [6]Instituto di Astrofisica Spaziale e Fisica Cosmica, CNR, Rome, Italy. [7]U.S. Geological Survey, Denver, CO 80225, USA. [8]NASA Ames Research Center, Moffet Field, Mountain View, CA, USA. [9]Institute of Planetary Exploration, German Aerospace Center, Germany. [10]Department of Earth and Space Sciences, University of Washington, Seattle, WA, USA. [11]Osservatorio Astronomico di Capodimonte, Via Moiariello 16, 80131, Napoli, Italy. [12]Department of Astronomy, Cornell University, Ithaca, NY, USA. [13]Laboratoire de Planétologie et Géodynamique, Université de Nantes, France. [14]U.S. Geological Survey, Flagstaff, AZ 86001, USA.